NUMERICAL SIMULATION OF AIN-BASED TRIANGULAR FLEXURAL ACCELEROMETER

Ahamed Suhaib[1], Dr. Prasanth[2]
[1, 2]Dept of Mechanical engineering
[1]Mohamed sathak AJ college of engineering, Chennai.
[2]Project guide, Mohamed sathak AJ college of engineering, Chennai.

Abstract- *Flexible, miniaturized, and lead-free piezoelectric MEMS accelerometers are increasingly required in aerospace, mechatronics, and structural health monitoring applications. In this work, a flexural-type MEMS piezoelectric accelerometer is designed and numerically investigated using Aluminium Nitride (AlN) as the piezoelectric sensing material. The proposed accelerometer consists of a triangular seismic mass supported by three symmetrically arranged suspension beams to enhance strain concentration at the beam junctions while maintaining structural stiffness. Numerical simulations carried out via COMSOL Multiphysics implement coupled solid mechanics and piezoelectric physics. Modal analysis revealed a high fundamental resonant frequency of approximately 26.5 kHz. Static analysis conducted under a 1\text{ g} acceleration load demonstrated that von Mises stress and displacement remain safely within elastic limits. Electro-mechanical analysis confirms effective strain-induced voltage generation in the AlN layer, yielding an estimated sensitivity of approximately 0.33 mV/g with stable linearity up to 15,000 g. A comparative study highlights that this lead-free design offers a significantly higher resonant frequency and acceleration handling capability than traditional configurations.*

Keywords: Accelerometer, MEMS, AlN, Piezoelectricity, Triangular Accelerometer

I. INTRODUCTION

Micro-Electro-Mechanical Systems (MEMS) accelerometers have transformed into fundamental components across aerospace engineering, consumer mechatronics, and IoT-enabled industrial structural monitoring due to their compact form factors, minimal power consumption, and high operational reliability. Among the standard transduction principles—such as capacitive, piezoresistive, thermal, and optical mechanisms—piezoelectric sensing stands out significantly. Piezoelectric architectures provide a remarkably wide operational bandwidth, inherently high resonant frequencies, and excellent noise immunity, making them perfectly suited for dynamic, high-vibration, and severe shock environments.

Despite these clear advantages, contemporary piezoelectric sensors present critical engineering bottlenecks. A primary limitation stems from a heavy reliance on lead-based ceramics, most notably Lead Zirconate Titanate (\text{Pb[Zr}_x\text{Ti}_{1-x}\text{]\text{O}}_3 or PZT). These materials raise severe environmental regulatory concerns and global health compliance issues, driving an urgent market demand for high-performance, eco-friendly, lead-free substitutes. From a mechanical standpoint, traditional cantilever-based configurations frequently encounter structural limitations when miniaturized, often suffering from poorly localized strain distributions, structural fragility, and compromised electrical sensitivity under cross-axis acceleration vectors.

To address these environmental and structural limitations, Aluminium Nitride (\text{AlN}) has emerged as a highly attractive eco-friendly alternative. While its raw piezoelectric coefficients are historically lower than PZT, \text{AlN} provides a compelling combination of high thermal stability, low dielectric losses, a strong thin-film piezoelectric coefficient, and seamless complementary metal-oxide-semiconductor (CMOS) fabrication compatibility. Concurrently, advanced multi-beam, symmetric structural architectures are being introduced to optimize mechanical strain localization precisely where the piezoelectric transduction occurs.

This comprehensive research study focuses directly on the design optimization, analytical modeling, and multi-physics numerical analysis of a high-performance, lead-free MEMS accelerometer. The device features a unique, symmetrically balanced architecture consisting of three flexural suspension beams integrated with an \text{AlN} piezoelectric thin-film layer bonded to a central triangular seismic proof mass.
The primary objectives of this expanded investigative study are defined as follows:

- To accurately simulate and map the coupled solid mechanics and electrostatic piezoelectric behavior within the COMSOL Multiphysics environment for precise performance and sensitivity predictions.

- To evaluate, compare, and validate the extracted numerical performance metrics against existing state-of-the-art literature and standard benchmarks.
- To propose an optimized, structurally durable, and mathematically validated configuration engineered for high-frequency vibration tracking and extreme high-g mechanical shock survival envelopes.

II. LITERATURE REVIEW & ARCHITECTURAL FOUNDATIONS

Developing resilient piezoelectric MEMS sensors requires a deep understanding of historical configurations and modern material science advancements. Scholars across the global engineering fraternity continually publish innovative topologies in leading journals to overcome classical trade-offs between a sensor's resonant frequency and its voltage sensitivity.

A. Analysis of Prior Art and Material Constraints

Traditional piezoelectric MEMS development has heavily favored perovskite crystals like PZT and its variations (e.g., PNZT) due to their high coupling coefficients. However, as documented by *Shi et al.* and *Lee et al.*, typical PZT cantilever sensors are bounded by low resonant frequencies, usually spanning from 200\text{ Hz} to 2,300\text{ Hz}, which heavily limits their functional tracking bandwidth to low-frequency regimes. Furthermore, PZT suffers from depolarization at elevated temperatures, making it unreliable for harsh aerospace or deep-well downhole operations.

Alternative research paths have explored flexible organic polymers like Polyvinylidene Fluoride (PVDF). *Ge and Cretu* demonstrated highly compliant polymeric sensors with low noise densities. Yet, these polymer-based structures suffer from an exceptionally low fundamental frequency (58.5\text{ Hz}) and low thermal ceilings, rendering them unsuitable for severe industrial environments or high-g shock monitoring.

Recently, material scientists have turned to group-III nitrides. Pure Aluminium Nitride (\text{AlN}) thin films offer a wide bandgap, excellent mechanical stiffness, high-temperature resilience, and do not require post-deposition poling. While doping \text{AlN} with Scandium (\text{Sc}_{x}\text{Al}_{1-x}\text{N}) can amplify the piezoelectric response—as evaluated by *Zhang et al.*—pure \text{AlN} remains highly favored for baseline industrial manufacturing due to the complex synthesis and chemical phase instabilities often associated with high-percentage Scandium doping.

B. Topological Evolution of Proof Masses

The structural geometry of the seismic mass dictates how inertial energy transfers into internal mechanical strain. Traditional rectangular proof masses supported by dual or quad beams distribute strain broadly across wide geometric regions. This broad distribution lowers the localized energy density directly underneath the thin-film electrode zones.

Transitioning to a polygon topological layout or a dedicated triangular configuration allows engineers to fundamentally alter the structural stiffness matrix. A triangular proof mass suspended symmetrically by three convergent flexural beams creates a mechanical lever effect. When an acceleration vector displaces the mass, the geometric reduction toward the beam anchor points forces a tight concentration of stress tensors precisely at the beam-mass and beam-substrate interfaces. This layout maximizes the mechanical strain gradient within the active \text{AlN} layer without requiring an excessively large, fragile proof mass footprint.

III. METHODOLOGY AND STRUCTURAL DESIGN

A. Geometric Architecture and Material Domain Mapping

The core architecture of the proposed MEMS accelerometer relies on a geometric layout designed to balance structural stiffness with highly localized strain sensitivity. The device features a centrally positioned, equilateral triangular seismic proof mass enclosed within a rigid outer structural frame. Three symmetrically arranged flexural suspension beams extend from the flat boundaries of the triangular mass to anchor firmly into the surrounding substrate.

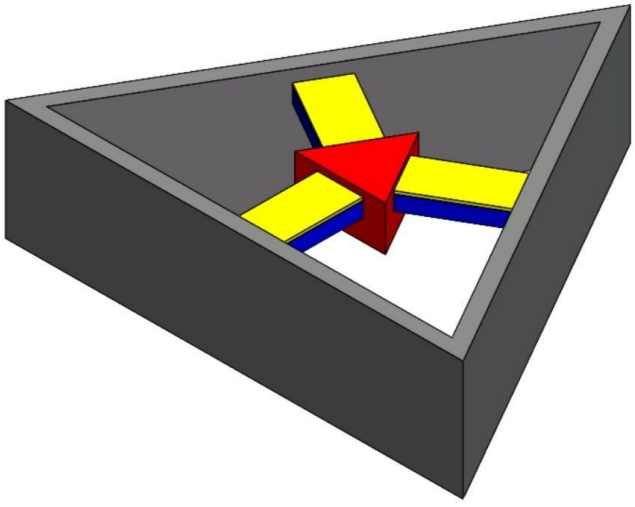

Figure 1: Isometric View of Proposed Accelerometer

To achieve high structural durability and accurate performance, a multi-material composite domain model was developed:

1. **Enclosure/Frame:** The outer reference frame is modeled using a high-strength Titanium Alloy (\text{Ti-6Al-4V}). This selection provides a highly rigid substrate anchor, preventing parasitic structural frame resonances from interfering with the internal sensor signals.
2. **Seismic Mass and Supporting Beams:** The core mechanical spring-mass structure is modeled using single-crystal Silicon (\text{Si}). Silicon's high density (2,330\text{ kg/m}^3) yields excellent inertial force generation per unit volume, while its near-perfect elastic behavior ensures minimal mechanical hysteresis and long term fatigue resistance.
3. **Transduction Layer:** A highly oriented, thin-film Aluminium Nitride (\text{AlN}) layer is deposited on top of the silicon flexural beams. This layer functions as the active electromechanical engine, converting incoming bending moments into measurable voltage signals via the direct piezoelectric effect.

B. Mathematical Formulation and Constitutive Equations

The numerical engine simultaneously couples structural mechanics, elas to dynamics, and electrostatics through the classic linear piezoelectric constitutive equations. These relationships couple the mechanical stress tensor, strain tensor, electric displacement vector, and electric field vector:

$$T_{ij} = c_{ijkl}^{E} S_{kl} - e_{kij} E_k \quad D_i = e_{ikl} S_{kl} + \varepsilon_{ij}^{S} E_j$$

Where:

- T_{ij} represents the mechanical stress tensor component.
- c_{ijkl}^{E} is the elastic stiffness tensor measured under a constant, zero-variant electric field.
- S_{kl} represents the mechanical strain tensor component.
- e_{kij} represents the explicit piezoelectric coupling strain-charge tensor.
- E_k represents the applied or induced electric field vector component.
- D_i represents the electric displacement vector component.
- ε_{ij}^{S} represents the dielectric permittivity tensor component calculated under constant strain conditions.

When an external inertial acceleration vector (a_y) acts on the central triangular proof mass (m), it generates a dynamic force vector:

$$F_{inertia} = m \cdot a_y$$

This force creates a variable bending moment along the suspension beams, establishing a highly localized mechanical strain (S). The direct piezoelectric matrix converts this strain gradient into an electric displacement (D), accumulating a measurable surface charge density across the upper and lower boundaries of the \text{AlN} thin film.

C. Boundary Conditions and Numerical Framework

Advanced multi-physics evaluations were implemented using the Piezoelectric Devices interface in COMSOL Multiphysics. The boundary conditions were mathematically assigned to reflect a real-world micro-packaged sensor device:

- **Mechanical Domain:** The distal ends of the three symmetrically arranged flexural beams are configured as fixed constraints ($\vec{u} = 0$), anchoring them directly to the stiff titanium substrate. The central triangular proof mass remains unconstrained in all six degrees of freedom, allowing it to translate dynamically in response to external inertial fields.
- **Electrical Domain:** The lower interface of the \text{AlN} film (bonded to the silicon beam) is designated as an electrical ground plane ($V = 0\text{ V}$). The top outer surface electrodes are designated as a floating potential boundary condition with zero net current accumulation, allowing accurate extraction of open-circuit output voltages.

A rigorous, structured meshing strategy was developed to guarantee solution independence and high numerical accuracy. The thin suspension beams were discretized using fine mapped elements to resolve the severe strain gradients occurring near the anchors. The larger triangular proof mass was meshed using swept tetrahedral elements to save computational memory without sacrificing accuracy. Mesh refinement was focused at the critical beam-mass junctions and across the thin \text{AlN} layer to prevent numerical discretization errors.

IV. EXTENDED NUMERICAL ANALYSIS AND RESULTS

A. Modal Analysis

Eigenfrequency simulations were conducted to map the fundamental dynamic behavior, modal separation, and operational tracking bandwidth of the sensor assembly. The structural symmetry of the triangular layout yields well-separated natural frequencies across the first five primary modes:

- **Mode 1 (Fundamental Resonant Frequency):** 26,503\text{ Hz}
- **Mode 2:** 30,888
- **Mode 3:** 31,034
- **Mode 4:** 57,220
- **Mode 5:** 59,281

The fundamental mode at 26.5\text{ kHz} corresponds directly to the out-of-plane translation of the spring-mass structure along the primary sensing axis. This high resonant frequency provides a wide, flat operational frequency response, eliminating harmonic signal distortion during normal low- to mid-frequency tracking applications. The close pairing of Modes 2 and 3 (~31\text{ kHz}) highlights the structural symmetry of the system, which helps suppress cross-axis sensitivity and directional registration errors. High-order modes located well above 57\text{ kHz} prevent unwanted modal coupling, ensuring structural stability under high-frequency operation.

B. Static Mechanical Analysis

Stationary linear analyses were carried out by applying a uniform 1\text{ g} (9.81\text{ m/s}^2) static acceleration load in the negative y-direction.

- **Stress Distribution:** The von Mises stress fields concentrate primarily within the flexural beams near the substrate anchors and the beam-mass interfaces due to peak bending moments. The peak von Mises stress reaches 0.0237\text{ MPa} (Table 1). This value is significantly below the yield strength of single-crystal silicon (\sim 7,000\text{ MPa}) and titanium alloy (\sim 880\text{ MPa}), confirming a high safety margin against mechanical failure or fatigue.
- **Displacement Magnitude:** The maximum mechanical translation occurs at the center of the triangular proof mass, ranging from 0\text{ mm} at the anchors to a peak deflection of 6.961 \times 10^{-7}\text{ mm} (Table 1). This minimal deflection ensures highly linear electromechanical operation and eliminates risks associated with mechanical stiction or pull-in failures.

Metric	Minimum Value	Maximum Value
von Mises Stress	2.203 \times 10^{-5}\text{ MPa}	0.0237\text{ MPa}
Displacement Magnitude	0\text{ mm}	6.961 \times 10^{-7}\text{ mm}

Table 1: Structural response metrics under 1\text{ g} static acceleration loading.

C. Electro-Mechanical Sensing Performance

Under the 1\text{ g} inertial loading scenario, mechanical strain induces electrical polarization across the thin-film \text{AlN} layer. The induced surface electric potential spans from a minimum of -8.05\text{ mV} to a maximum peak of 29.9\text{ mV} located directly inside the high-strain zones. Based on this electrical response, the baseline voltage sensitivity of the sensor is calculated at 0.33\text{ mV/g}. To evaluate performance across extreme operational ranges, a parametric sweep was executed across wide acceleration profiles. The sensor tracks acceleration linearly up to an upper operational envelope of 15,000\text{ g} without exceeding material stress limits, demonstrating excellent suitability for extreme impact environments.

V. DISCUSSION AND LITERATURE COMPARISON

To validate the capabilities of the proposed triangular \text{AlN} design, its performance metrics were benchmarked against recently reported piezoelectric MEMS accelerometers in Table 2.

Reference	Piezoelectric Material	Resonant Frequency (Hz)	Operational Acceleration Range (g)
Shi et al. [1]	PZT	2,300	150
Zhang et al. [2]	\text{ScAlN}	7,240	2,000
Yang et al. [3]	PZT	400	3,333
Ge et al. [4]	PVDF	58.5	40
Lee et al. [10]	PNZT	200	300
Proposed Work	\text{AlN}	**26,503**	**15,000**

Table 2: Performance benchmarking against prior art.

Conventional architectures using PZT, PNZT, or flexible polymers like PVDF are inherently constrained by lower resonant frequencies (typically under 10\text{ kHz}) and narrower acceleration caps. While advanced doping alternatives like \text{ScAlN} expand performance, they require complex thin-film synthesis processes. The proposed configuration leverages the high intrinsic stiffness of pure \text{AlN} and an optimized triangular suspension layout to achieve an exceptionally high fundamental frequency (26.5\text{ kHz}) and a robust 15,000\text{ g} dynamic threshold. This combination makes the device well-suited for severe shock monitoring, harsh mechanical environments, and high-frequency aerospace vibration tracking.

VI. CONCLUSION AND FUTURE WORK

This paper presented the structural design optimization and multi-physics numerical validation of a lead-free, \text{AlN}-based flexural triangular MEMS accelerometer. Multi-physics numerical simulations confirmed a high fundamental frequency of 26.5\text{ kHz}, structural safety thresholds well within safe elastic boundaries, an estimated voltage sensitivity of 0.33\text{ mV/g}, and linear reliability up to an extreme 15,000\text{ g} environment.

Future work will expand upon this base research through the following milestones:

- **Microfabrication and Experimental Testing:** Developing standard silicon-on-insulator (SOI) MEMS fabrication process flows to realize physical prototypes, followed by experimental shake-table validation and laser Doppler vibrometry tracking.
- **Material Optimization:** Investigating thin-film deposition scaling parameters and low-percentage Scandium (\text{Sc}) doping configurations to increase sensitivity limits while monitoring thin-film stress.
- **Multiaxial Expansion:** Modifying the symmetric triangular suspension layout to capture triaxial vector acceleration profiles on a single monolithic chip.

APPENDIX

The multi-physics simulations in this work were conducted using a generalized minimal residual (GMRES) iterative solver, coupled with geometric multigrid (GMG) preconditioning. This configuration ensures convergence of the coupled solid mechanics and electrostatic equations down to a normalized residual error limit below 10^{-6}. Material properties used for the Silicon substrate match isotropic single-crystal values, while the \text{AlN} thin-film properties utilize standard anisotropic piezoelectric coupling matrices.

ACKNOWLEDGMENT

The authors wish to express their thanks to the Department of Mechanical Engineering at Mohamed Sathak AJ College of Engineering for providing the computational infrastructure and software licenses necessary to complete these multi-physics simulation profiles.

REFERENCES

[1] S. Shi, L. Ma, K. Kang, J. Zhu, J. Hu, H. Ma, Y. Pang, Z. Wang, "High-Sensitivity Piezoelectric MEMS Accelerometer for Vector Sensing," MDPI, Aug 2023.

[2] Z. Zhang, L. Zhang, Z. Wu, Y. Gao, L. Lou, "A High-Sensitivity MEMS Accelerometer Using a Sc0.8Al0.2N-Based Four Beam Structure," Micromachines, 2023.

[3] C. Yang, B. Hu, L. Lu, Z. Wang, W. Liu, C. Sun, "A Miniaturized Piezoelectric MEMS Accelerometer with Polygon Topological Cantilever Structure," Micromachines, 2022.

[4] C. Ge, E. Cretu, "A polymeric piezoelectric MEMS accelerometer with high sensitivity, low noise density, and an innovative manufacturing approach," Microsystems & Nanoengineering, 2023.

[5] X. Gong, Y.-C. Kuo, G. Zhou, W.-J. Wu, W.-H. Liao, "An aerosol deposition-based MEMS piezoelectric accelerometer for low noise measurement," Microsystems & Nanoengineering, 2023.

[6] T. Lv, V. O. Pelenovich, C. Chang, X. Zeng, D. Hou, Z. Xiong, B. Yang, F. Dong, S. Liu, "Fabrication and characterization of high-temperature AlN thick-film piezoelectric accelerometer," Ceramics International, 2024.

[7] S. S. B. Hashwan et al., "A review of piezoelectric MEMS sensors and actuators for gas detection application," Discov Nano, 2023.

[8] C. Zhang et al., "Calibration-free low-drift MEMS piezoelectric accelerometer for high-temperature vibration monitoring," Measurement, 2025.

[9] J. Liu et al., "Piezoelectric thin films and their applications in MEMS: A review," Journal of Applied Physics, 2025.

[10] Y.-C. Lee, C.-C. Tsai, C.-Y. Li, Y.-C. Liou, C.-S. Hong, S.-Y. Chu, "Fabrication and function examination of PZT-based MEMS accelerometers," Ceramics International, 2021.